Chapter 7

GLOBAL WARMING IMPACT ON RIVER THERMAL PATTERN IN FUTURE

7.1 Introduction

Increased levels of carbon dioxide and radioactive trace gases have been observed in the atmosphere of the earth over the last few decades. The excessive levels of these gases have been one of the many reasons for greenhouse warming and climate change (Jiang et al., 2007). It has been inferred unanimously that throughout the 20^{th} century, the average global air temperature has tended to increase, especially during the last 15-20 years. The scientific community across the globe has given significant attention to climatic variability. An effective water management system depends to a large extent on a well-functioning institutional framework, which is a prerequisite for adaptation to the contemporary climate variability uncertain climate change scenarios. All the facets of the environment can get disrupted by the ill-effect of adverse climate change. The bonding between the biotic and abiotic components of the ecosystem gets disrupted very badly (Jain and Singh, 2020). Due to the consequence of global warming environment has been destabilizing at an alarming pace, like the melting of glaciers and ice (Dyurgerov and Meier, 2000; Gregory et al. 2004) the rise of the sea level (Ramachandran et al. 2017), the occurrence of cyclones, floods, etc. becoming more intense and frequent (Easterling et al. 2000; Majumder et al. 2017) and the disruption in the agricultural pattern can also transpire (Mall et al. 2006). Needless to say that climate is the most important

factor which determines the pattern of land utilization. It strongly influences human activity.The attributes of climate i.e., rainfall, temperature, wind velocity, and humidity, have a good affinity with the agricultural pattern. Since crop-producing ability of an area depends largely upon climatic and soil conditions, the role of these elements can not be ignored to ascertain the agricultural activities. Some studies have indicated that the one million people residing in the mega deltas of the world like the Ganga-Brahmaputra delta, Nile delta, and Mekong delta will be directly affected due to coastal erosion, sea-level rise, flooding, and land loss by the year 2050 (McCarthy et al., 2001; Ericson et al. 2006). The menace of global warming-induced climate change affects almost all the ecosystems around the globe. The aquatic ecosystem has been one of them, and it is liable to be vulnerable to the disturbances induced by climate change. The river ecosystem can be directly and indirectly impacted by the combining effect of climate change as well as the other stressors (Durance and Ormerod, 2009; Jain and Singh, 2020). These impacts affect the dynamics and hydrology of the aquatic ecosystem and different species living in the ecosystem. Climate change affects river water resource management (Middelkoop et al. 2001; Alcamo et al. 2007), river water quality (Delpla et al.2009; Whitehead et al. 2009), eutrophication (Rabalais et al. 2009; O'Neil et al. 2012). On the other hand, efficiencies of water resource management could be improved considerably, thereby reducing vulnerability by adopting many of the sensible institutional, legal and economic measures that are considered to be an integral part of a viable 'no regrets' adaptation strategy promoted by UNDP, world bank and IPCC (Stakhiv, 1998). Since the late 19^{th} century, the global climate has warmed by about 0.05°C. During the last two decades, climatologists have attributed a distinct trend of increasing global air temperature to growing atmosphere CO_2 and other 'greenhouse' gases. Of great scientific and practical interest is studying the river

flow response to rising global air temperature in different regions of the world. Studies on river flow dynamics can be useful with revealing the 'CO_2 signals' as charging water content is a good climate indicator (Georgryevsky, 1998). The river geomorphology along with the associated land-use pattern in the river basin also gets affected due to climate change (Boon and Raven, 2012; Oliver and Morecroft, 2014). Changing climatic conditions will obviously result in changing water resources in the river basin, regions, and countries. The direction of these changes will determine the general strategy of population and economy in the 21st century (Georgiyevsky, 1996). Most of the rivers of the world have been assimilating an adverse impact due to global warming and climatic change. The Nile, Amazon, and Yangtze rivers are vivid examples. The change in the climatic pattern over the river basin has influenced the aquatic ecosystem (Pletterbauer, 2018). Keeping this in view, the study of the climatic change-induced riverine bodies is of utmost significance.

Rivers have been considered as the lifeline of the nations like India. Indian rivers are the primary source of irrigation for the agricultural sectors in the country on which approximately 70% of the population depends for livelihood. Apart from this, rivers have also been a significant source of potable water, transportation, hydropower generation, aquaculture, etc. (Jain and Singh, 2020). Unfortunately, the pristine value of our river ecosystem is on the verge of peril. On the other hand, demands for freshwater will continue to grow, but the resource is limited. The limited resource is assimilating the threat of global climate change. Climate change also has an impact on all the Indian rivers. Some scientific studies have indicated that climate change affects the rivers by altering the rainfall pattern, raising the water temperature along with the air temperature, increasing the evaporation rate, and changing the groundwater table. Although small changes in climatic characteristics significantly impact the availability

of water resources and their use, yet no proper study on the Ganga river in this direction has been made. There are 22 river basins in India, and among them, the Ganga river basin is the largest and most significant (Jain and Singh, 2020). In its journey of 2525 km from its source to sea, the river passes through the three most populous states viz. Uttar Pradesh (UP), Bihar, and West Bengal (WB); however, its drainage basin (861,404 sq. km) also encompasses Punjab, Himachal Pradesh (HP), Rajasthan, and Madhya Pradesh (MP). Its basin is the seat of nearly 37% of the country's population. The river Ganga is one of the most important rivers of the country, and no wonder that it served as the cradle of the Indian civilization. Several important industrial and cultural cities have been situated along its bank. This river supports the livelihood of millions of people as nearly 670 million people live in the plains of river Ganga (Whitehead et al. 2015). To intensify the Ganga rejuvenation efforts and create more consciousness regarding the prevention of pollution, the River Ganga has been affirmed the status of 'National River of India' in November 2008. Several national-level programs like *Namami Gange* and National Mission for Clean Ganga have been launched. The Indian government has also created organizations like the National Ganga River Basin Authority to revive the river. Before that, the then Central Board for Prevention and Control of water pollution (now Central Pollution Control Board) in the nineties decided to undertake an integrated study of the entire Ganga basin covering all relevant aspects of water quality appraisal within the whole extent of the basin. But the resurrection of the river has not gone well according to the plan (Das and Tamminga, 2012). In such desperate situations, the influences of climate change may prove to be a significant setback for the river rejuvenation process. The Indian subcontinent has shown an increasing trend in temperature over the last 120 years. In the 20th century, the average temperature of the Indian subcontinent had been

raised by 0.48°C (Singh and Kumar, 2018; Jain and Singh, 2020). As drier atmospheric scenarios will lead to the more intensified drying of the land surface, it will put an extra burden on the river to accomplish the water demand. The Ganga river basin has already been placed in the water stress region (Singh and Kumar, 2018). The rise in the air temperature also inflates the water surface temperature of the streams. Some models have predicted that the surface water temperature of the Ganga river has been expected to rise by 1-4°C between the year 2010 to 2050 (Moors et al. 2011). The increase in the river water temperature also affects the river's water quality. For delineating the river thermal pattern along with river water quality assessment, remote sensing technology has been much more effective (Ling et al. 2017; Yigit Avdan et al. 2019). Compared to traditional methods, remote sensing datasets can provide the synoptic view, repetitive coverage of a particular place to observe the change, and information other than visible wavelengths, which has been otherwise impossible to detect through the naked eyes. Time series-based studies can be very conveniently performed using this technology (Budd et al. 2001; Roy et al. 2017; Das et al. 2021). The Seasonal Autoregressive Integrated Moving Average (SARIMA) and the Prophet model have been used for future prediction by some researchers (Chikkakrishna et al.2019; Samal et al.2019). These models are machine learning (ML) based models (Vishwakarma et al.2020). Researchers have also used the Long Short Term Memory (LSTM) technology for future time stamp forecasting (Elsworth and Güttel,2020) using remote sensing datasets. The LSTM is a type of deep learning-based model, and these models have been robust to the outliers, non-linearity, and noise (Kong et al. 2018).

In the present chapter, satellite-based datasets for the period of 2000-2020 for the river thermal pattern analysis and air temperature pattern assessment have been elaborated. The nighttime

satellite images have also been analyzed in this work to dissect the urban sprawl over the region. Future trend forecasting for air temperature has been done with the SARIMA and Prophet models. The LSTM model has been used to predict the river thermal pattern and urban sprawl. To the best of our knowledge, this has been the first attempt to predict the river thermal pattern, and urban sprawl using the LSTM model. The objective of the present work is to delineate the impact of human-induced climate change on the water resources of the river Ganga in Varanasi, an important segment in the study stretch, in the future years (2022 and 2025). The study region has been done is shown in figure 7.1. The region has been divided into two stretches: the city river stretch and the non-city river stretch. The river temperature estimation and analysis have been done for the two stretches separately. In the location map of the study area, the river shapefiles have been placed over the true color composite of the Sentinel-2 satellite imagery. The Sentinel-2 image has a spatial resolution of 10 meters.

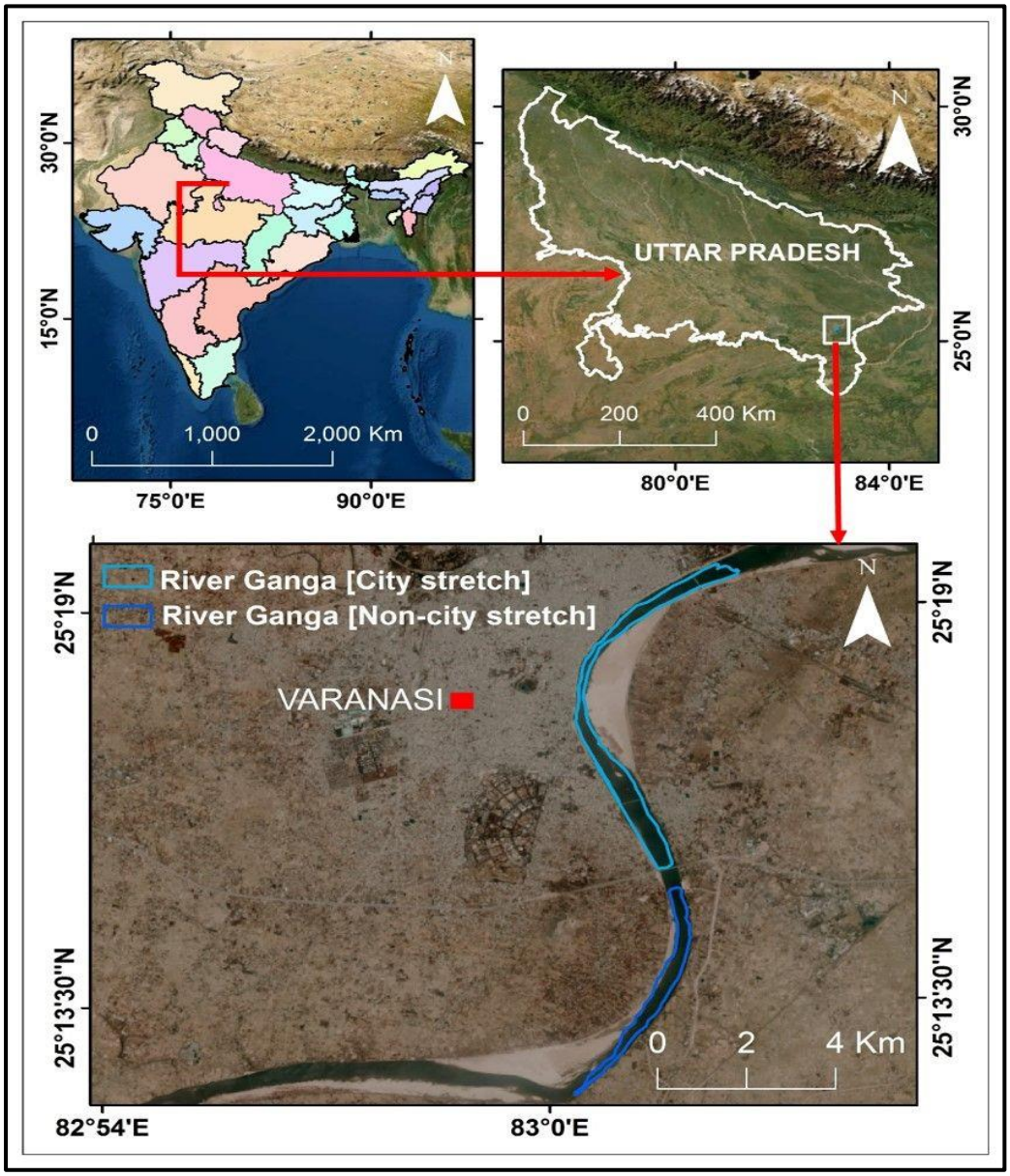

Figure 7.1 Geo-location map of the region for which the work has been done

7.2 Data

7.2.1 LANDSAT datasets

Landsat-5, Landsat-7, and Landsat-8 satellite datasets have been used to assess the river temperature for the years 2022 and 2025. Only the December month imageries have been chosen in this work, and the first image has been of December 2000. For the years 2014 and 2019, no December month images have been available for the study stretch due to clouds, so November month images have been considered for these two years. December month has been chosen only because of the 21-year time span (2000-20); December month has the highest number of available images, i.e., 34. For other months, less number of images were available. All the datasets used for temperature have been processed in Google Earth Engine (GEE) platform, and these datasets have been marked as Level 1TP products. GEE provides *Surface Reflectance Tier 2* data, and these datasets consist of atmospherically corrected surface reflectance and brightness temperature values. The atmospheric correction has been done by using Land Surface Reflectance Code (LaSRC) algorithm (Vermote et al. 2016). In this study, after the year 2012, for all the next upcoming years, L-8 datasets have been considered. The summary of the Landsat imageries used for this study has been tabulated in Table 7.1.

Table 7.1 Summary of the Landsat datasets used in this study

Datasets	Dates	Description
Landsat-5	December 2004 to December 2010 (n=9)	Visible-Near Infrared optical imagery (30 m) and Thermal Infrared imagery (120m)
Landsat-7	December 2000 to December 2012 (n=13)	Visible-Near Infrared optical imagery (30 m) and Thermal Infrared imagery (60m)
Landsat-8	December 2013 to December 2020, November 2014, and 2019 (n=14)	Visible-Near Infrared optical imagery (30 m) and Thermal Infrared imagery (100m)

7.2.2 ERA 5 datasets

The description of this data has been given in Chapter 6. Air temperature datasets have been incorporated in this study for the period of January 2000 to June 2020. For each of the months, the air temperature has been calculated.

7.2.3 Visible Infrared Imaging Radiometer Suite (VIIRS) Day/Night Band (DNB) datasets

These datasets have been composited on a monthly basis. Cloud cover in these datasets has been determined using the VIIRS Cloud Mask product (VCM). Additionally, the data near the edges of the satellite swath have not been included in the generation of the composites. Data impacted by stray light, cloud cover, lightning, and lunar illumination have been filtered out before averaging. The nighttime image gives a rough estimate of the urban sprawl (Elvidge et al., 2017). The *avg_rad* band of the satellite has been used, having unit as nanoWatts/cm^2-sr. The average radiance for a particular month will be made available on the first day of the

following month. So, the average radiance of December will be made available on the first day of January next year. VIIRS images used in this study have been tabulated in Table 7.2.

Table 7.2 VIIRS Satellite image acquisition dates

VIIRS image acquisition dates
1-Jan-2014
1-Jan-2015
1-Jan-2016
1-Jan-2017
1-Jan-2018
1-Jan-2019
1-Jan-2020
1-Jan-2021

7.2.4 In-situ datasets

The in-situ datasets were collected on 14 December 2020. The river temperature has been recorded by using YSI ProDSS Water Quality Meter. This instrument has also saved the corresponding GPS location of the in-situ points. For the city stretch, 25 points, and for the non-city stretch, 15 points have been measured. The in-situ datasets have been further correlated with the L-8 satellite-generated datasets of 14 December 2020.

7.3 Methodology adopted for this work

7.3.1 Air temperature calculation using ERA 5 Datasets

The air temperature estimation has been done with the band *mean_2m_air_temperature,* which gives each day's average air temperature value. The band that gives the air temperature's

average value has been chosen. It has been done because the LANDSAT acquisition time for the study stretch has been approximately 10:30 AM IST, and the average temperature for each day occurs around 11:00 AM (Das et al. 2021). The city stretch of the river contains one ERA5 pixel, and the non-city stretch also contains a single ERA 5 pixel. The city and non-city pixels have different values. For city stretch and for each day, a single average value has been estimated. For the month for this particular stretch, there will be either 28, 29 (February leap year),30, or 31 values. Box plots have been made for each month's value for all the years under consideration. A similar procedure has been followed for the non-city stretch of the river as well.

River thermal pattern calculation using the LANDSAT satellite has been described in Chapter 3.

7.3.2 Future prediction of parameters

7.3.2.1 Air temperature prediction using SARIMA model

The ARIMA model can be incorporated for data forecasting. The general notation for the ARIMA model has been ARIMA (p; d; q), where p is the number of autoregressive (AR) terms, d is the order of differencing, q is the number of moving average (MA) terms (Wang and Guo, 2009; Kulkarni et al. 2018). The ARIMA model has been formulated (Samal et al. 2019) as:

$$\left(1 - \sum_{i=1}^{p} \phi_i L^I\right)(1 - L)^d X_t = \delta + \left(1 + \sum_{i=1}^{q} \theta_i L^I\right)\varepsilon_t$$

(7.1)

where L has been denoted as the lag operator, ϕ_i is the moving average part parameter, and ε_t is the error term. When the time series data display the seasonality feature, the SARIMA model has been used instead of the ARIMA. Mathematically, the SARIMA model can be denoted as

ARIMA (p; d; q) (P; D; Q)S where P, D, Q, and S have been corresponding to the seasonal AR order, seasonal differencing, seasonal MA order, and time span of repeating seasonal pattern respectively (Samal et al. 2019). The SARIMA can be shown in simpler terms without the differencing part (Wang and Guo, 2009; Lee et al. 2012) as:

$$\phi_p(B)\alpha_p(B^S)(1-B)^d(1-B^S)^D Y_t = \theta_q(B)\gamma_Q(B)^S\varepsilon_t \quad (7.2)$$

where, ϕ_p(B) = $1-\phi_1 B^1-\phi_2 B^2-\cdots-\phi_P B^P$, α_p(B) = $1-\alpha_1 B^S-\alpha_2 B^{2S}-\cdots-\alpha_p B^{pS}$

θ_q(B) = $1-\theta_1 B^1-\theta_2 B^2-\cdots-\theta_q B^q$, γ_Q(B) = $1-\gamma_1 B^S-\gamma_2 B^{2S}-\cdots-\gamma_Q B^{QS}$

7.3.2.2 Air temperature prediction with Prophet model

Facebook (a social networking giant) has developed the Prophet model (Taylor 2019). Due to the highest order accuracy, this model has been one of the better models for forecasting any trend or pattern. This model can be expressed as (Samal et al. 2019):

$$y(t) = g(t) + s(t) + h(t) + \in_t \quad (7.3)$$

where the model parameters g(t), s(t), h(t), $\in_t$ are piecewise linear curves for evaluating the non-periodic changes in time series, periodic changes, the effects of holidays with irregular schedules, error term accounts for any unusual changes not accommodated by the model respectively. The Fourier series has been used to make the proposed model fit for the seasonality effects and forecast based on it. Seasonal effect s(t) can be represented as (Borowik et al. 2018) :

$$s(t) = \sum_{n=1}^{N} a_n \cos\left(\frac{2\pi nt}{P}\right) + b_n \sin\left(\frac{2\pi nt}{P}\right) \quad (7.4)$$

where P represents the regular period.

These two models in this analysis have predicted the air temperature values. Root Mean Square Percent Error (RMSPE) (Lu and Kao, 2016) has been chosen to measure the performance of these two models' time series analysis and forecasting ability. The RMSPE has been calculated as:

$$RMSPE = \sqrt{\frac{1}{n}\sum_{i=1}^{n}\left(\frac{X_{est}-X_{act}}{X_{act}}\right)^2} \times 100 \quad (7.5)$$

where n represents the number of samples, X_{est} represents the value generated from the model, and X_{act} is the actual value obtained from the satellite data.

7.3.2.3 River temperature and nighttime radiance prediction

In this study, river temperature and nighttime radiance future values have been predicted using the LSTM algorithm. Using the past dataset, this model has been trained to find a pattern for a particular parameter at time t_i and its n preceding values $t_{i-1}, t_{i-2}, \ldots, t_{i-n}$ (known as time-window). The prediction of the future has been made on previous n values with the help of the identified patterns.

The LSTM has been termed as one of the variations of Recurrent Neural Network (RNN). The RNN has been developed by Sepp Hochreiter and Jürgen Schmidhuber in 1997. This model has the ability to learn long-term dependencies, and it can work reasonably well over a different variety of problems (Xiao et al. 2019). In the RNN architecture, hidden layers have been treated as the successive recurrent network. This structure can be opened to generate the outputs of a neuron constituent pattern at distinct time steps corresponding to the input time sequence. With this type of architecture, the RNN model has a strong ability to capture the previous knowledge

implanted in the past components of the input for an amount of time (Bengio et al. 1994). The diagrammatic sketch of the RNN unfolding structure is shown in figure 7.2.

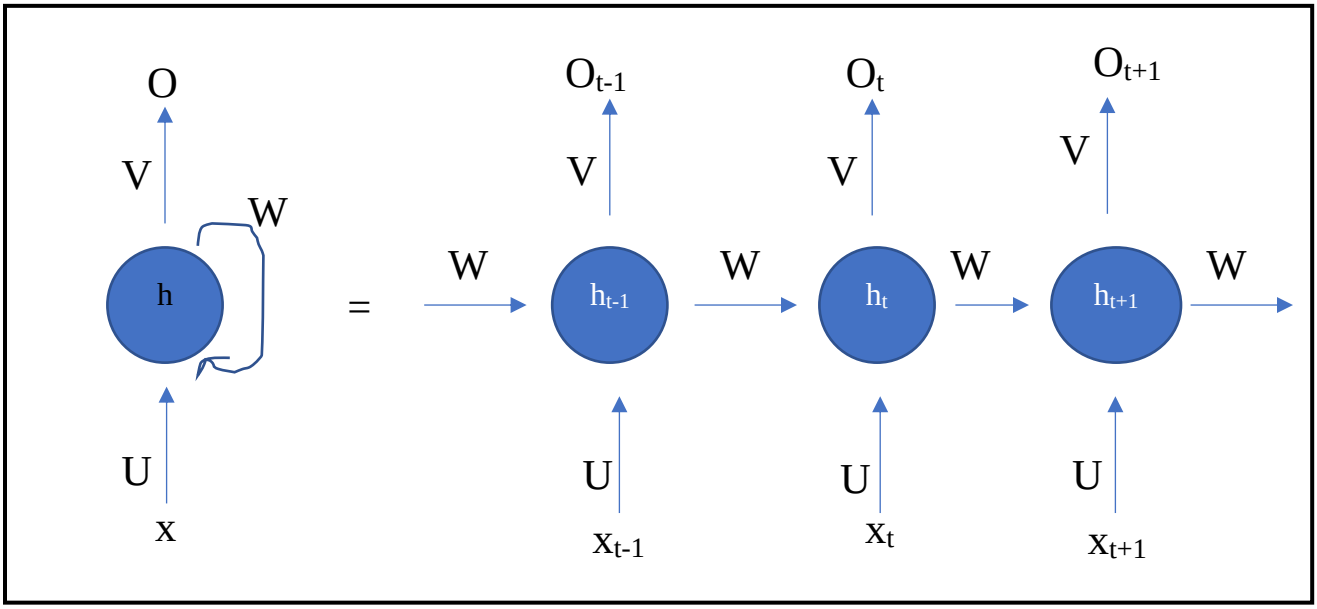

Figure 7.2 Unfolding structure of RNN

The steps of carrying forward can be explained mathematically

$$h_t = \sigma(Wx_t + Uh_{t-1} + b^{(h)}) \tag{7.6}$$

$$O_t = \sigma(Vh_t + b^{(0)}) \tag{7.7}$$

where x_t has been termed as input vector, h_t has been indicated as hidden state corresponding to x_t, O_t has been defined as output vector. U, V, and W have been the weight matrices. σ has been denoted as activation function, and *b* has been represented as bias vector.

The RNN architecture can forecast the next time step for the time-series datasets. It has been challenging to train RNN through the backpropagation technique for long time-series-based datasets. At each time step, the shrinkage or growth of the backpropagation gradients can get accumulated. Due to this accumulation, the gradients may vanish or explode over many time steps (Kong et al., 2018). The LSTM has been introduced to overcome this problem of vanishing or explosion. Information can be gathered from inputs for a long duration using a distinctive hidden unit, known as the LSTM cell, instead of the simple RNN unit [the blue node h in figure 7.2]. This study incorporates the LSTM structure given in Kong et al. (2018). The LSTM structure has been represented in figure 7.3.

It contains several gates, namely, the input gate (i_t), the output gate (o_t), the input modulation gate (m_t), and forget gate (f_t) along with the hidden state (h_t), and the memory cell (c_t). The gates have been computed by the following equations:

$$i_t = \sigma(W^{(i)}x_t + U^{(i)}h_{t-1} + b^{(i)}) \tag{7.8}$$

$$o_t = \sigma(W^{(o)}x_t + U^{(o)}h_{t-1} + b^{(o)}) \tag{7.9}$$

$$m_t = tanh(W^{(m)}x_t + U^{(m)}h_{t-1} + b^{(m)}) \tag{7.10}$$

$$f_t = \sigma(W^{(f)}x_t + U^{(f)}h_{t-1} + b^{(f)}) \tag{7.11}$$

where h_{t-1}, x_t has been denoted as previous hidden state and input vector, respectively. σ has been termed as logistic sigmoid function, *tanh* has been defined as the hyperbolic tangent function, and *b* has been indicated as bias vector. U and W have been the weighted matrices.

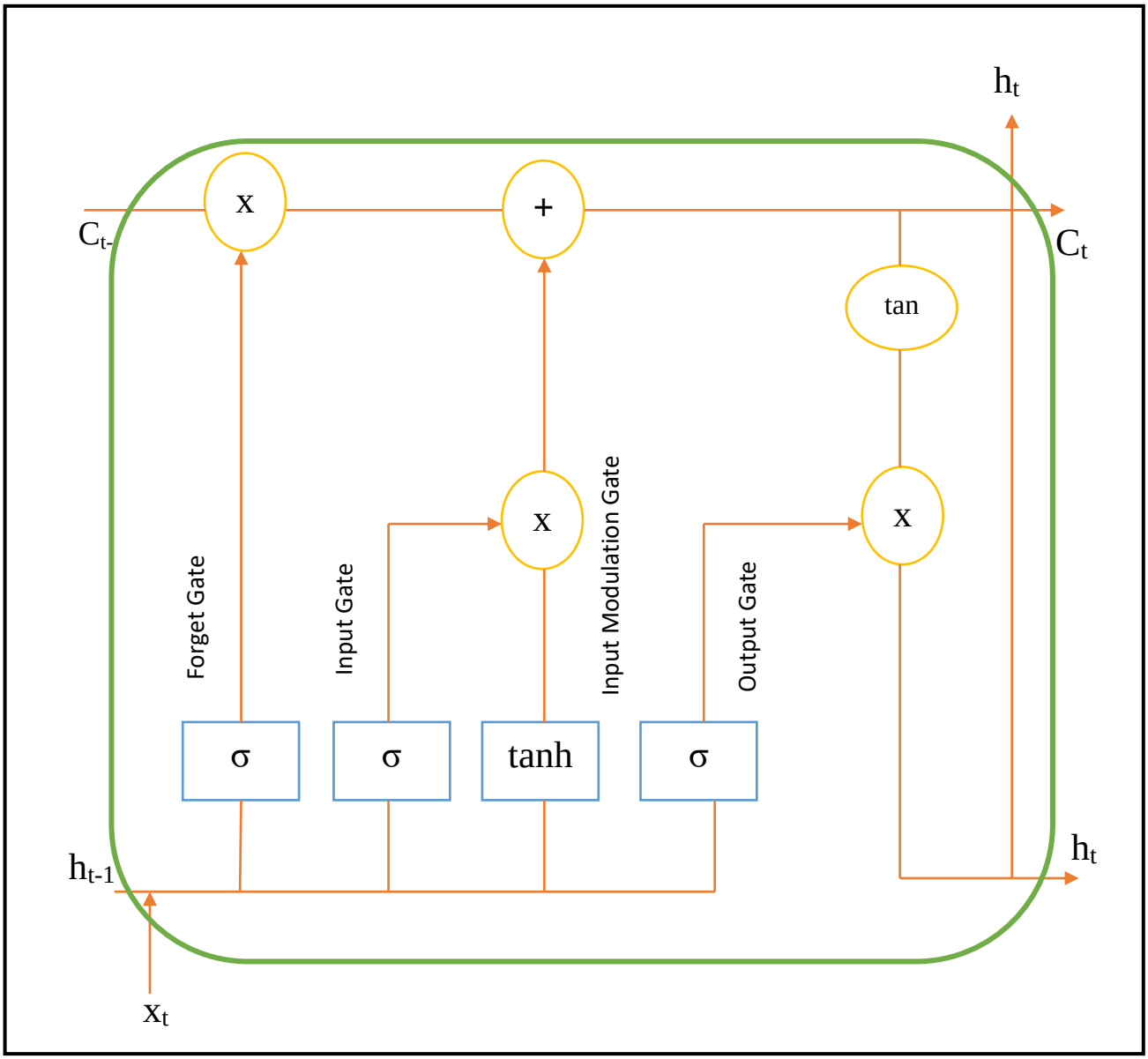

Figure 7.3 LSTM cell structure

The gates described in figure 7.3 have been used to calculate the h_t and c_t values as follows:

$$h_t = o_t . \tanh(c_t) \quad (7.12)$$

$$c_t = i_t . m_t + f_t c_{t-1} \quad (7.13)$$

" ." indicates pointwise multiplication of the two vectors. The c_t constitutes two components, namely previous memory cell (c_{t-1}) information modulated by the forget gate (f_t) and current input vector (x_t) information along with the preceding hidden state (h_{t-1}) modulated by the m_t. The LSTM network selectively forgets its preceding memory due to the forget gate. The LSTM network considers the current input because of the input gate. The information of the input gate has been modulated by the input modulation gate (m_t). The transfer of the information from the memory cell (c_t) to the hidden state (h_t) has been controlled by the output gate (o_t). The LSTM has the ability to learn the variations in the time series, and then it can make predictions based on those learnings.

The satellite images for river temperature have 36-time steps, and nighttime images have 9-time steps. For the LSTM model applied on thermal data, river temperature has been used as the sole input to the model. Similarly, the average radiance values have been inserted for the nighttime models. The minimum-maximum scaling techniques have been applied to the input datasets for the normalization procedure. The data normalization has been done to prevent the sudden gradient changes and to smoothen the convergence (Yussof et al. 2021). The LSTM can only predict one-time step at a time. The output y_{t+1} has been predicted using an input sequence (x_{t-l+1},…,x_{t-1}, x_t) where *l* is the step sliding time window. Similarly, the output y_{t+n} using an input sequence (x_{t+n-l},…, x_t, y_{t+1}, …, y_{t+n-1}). The Rectified Linear Unit (ReLU) activation function has been used for this analysis. Unit number 64 has been implemented;

after that, a dropout layer with a rate of 0.001has been given to the LSTM network to prevent the network from overfitting and underfitting. The model has been compiled with RMSPE loss function, and an adaptive gradient algorithm (AdaGrad) optimizer with a learning rate of 0.01 has been implemented in this model. It is well-suited when dealing with sparse data. It will optimize the hyperparameters like learning rate, epoch count, and the number of hidden layers. The fundamental function of parameter update is

$$\Theta_{t+1} = \Theta_t - \frac{\alpha}{\sqrt{\varepsilon + \sum g_t^2}} \odot g_t \tag{7.14}$$

where Θ_t is a parameter at time t, α is the learning rate, g_t depicts gradient estimate, ε is the smoothening term that avoids division by zero, and $\odot$ refers to element-wise multiplication (Venkatesh and Jeyakarthic, 2020).

This study uses the LSTM model to predict the future river temperature and average nighttime radiance for the study stretch for 2022 and 2025.

7.4 Results

7.4.1 Statistics for the in-situ measurements and satellite data validation

The in-situ measurement was done on 14 December 2020. The temperature has been negatively skewed. The river temperature ranges between 16.06-20.63°C having a median value of 19.69°C. December lies in the winter season, so the river temperature has been hovering around these ranges. The statistical values for the river temperature have been given in Table 7.3.

Table 7.3 Descriptive statistical values of in-situ river temperature

Parameters	Temperature
Number of Samples	40
Median	19.69°C
Standard Deviation	0.71°C
Variance	0.51°C
Skewness	-2.97
Kurtosis	13.28
Maximum	20.63°C
Minimum	16.06°C

The scatter plot between the in-situ measurements and satellite-derived datasets has been plotted. The RMSPE value for the river temperature has been 4.95%.

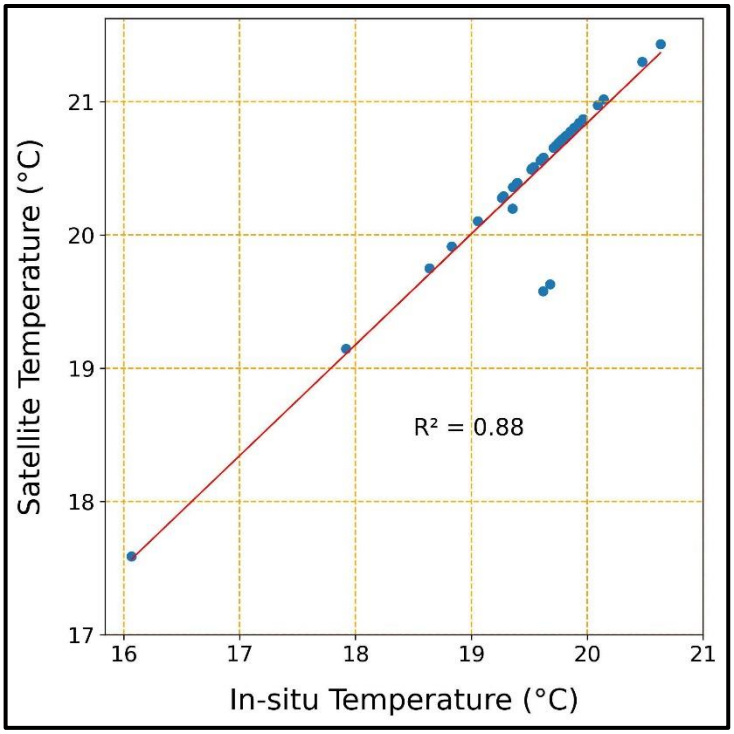

Figure 7.4 Scatter plot showing the relation between in-situ and satellite observed temperature

7.4.2 Air temperature pattern and future trend

The average air temperature pattern for the city and non-city river stretch both have shown an increasing tendency from 2015 onwards. The increasing mode has an effect on the forecasted temperature as well. For the city river stretch, the air temperature has been around 17°C for 2022, increasing to 19°C for December 2025. Similarly, for the non-city river stretch, the average air temperature for December 2022 hangs around 16.5°C, and it inflates to approximately 18.5°C for December 2025. The air temperature values have been predicted from 2021 onwards. The blue and red dots have been placed over the SARIMA and Prophet model graphs to indicate the above-mentioned values. Figures 7.5, 7.6 represent the future city

river stretch air temperature, and 7.7 and 7.8 represent the future non-city river air temperature pattern.

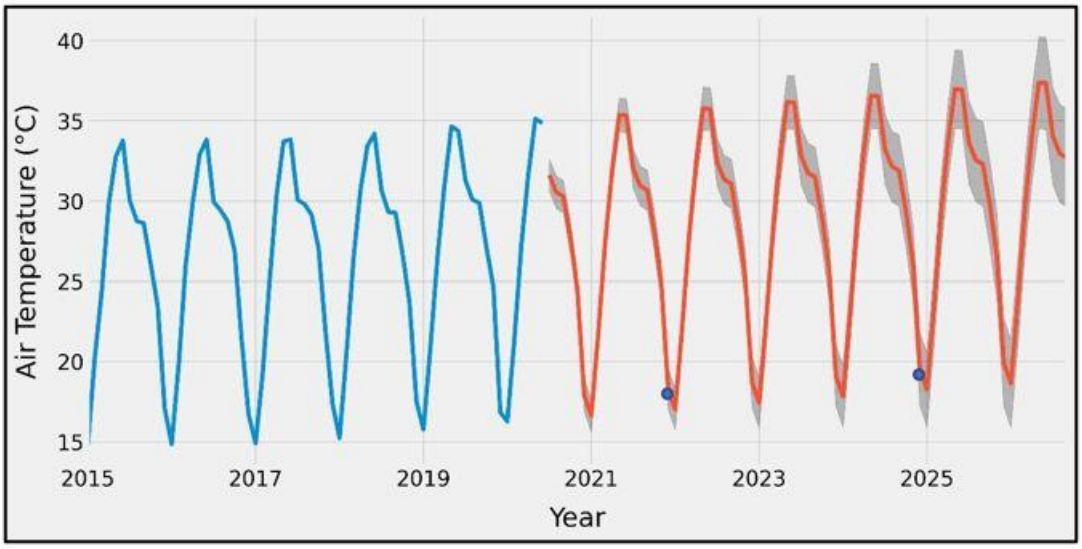

Figure 7.5 Sarima model predicted air temperature for the city river stretch

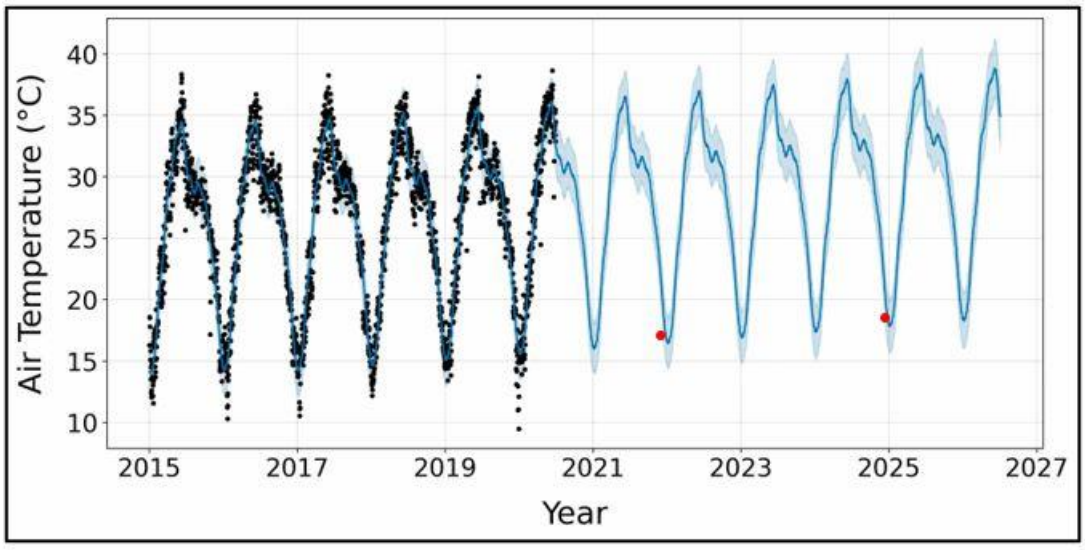

Figure 7.6 Prophet model predicted air temperature for the city river stretch

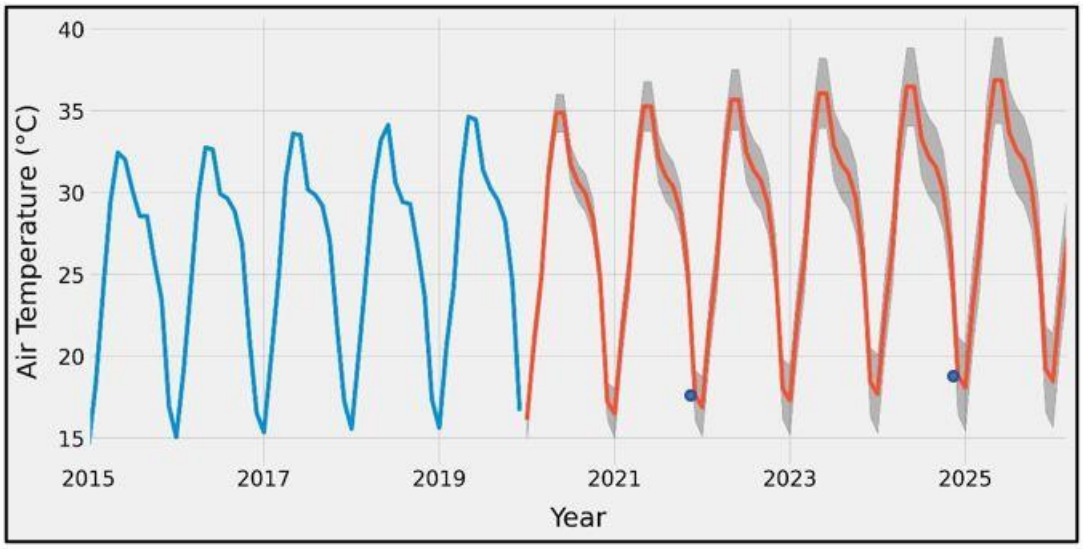

Figure 7.7 Sarima model predicted air temperature for the non-city river stretch

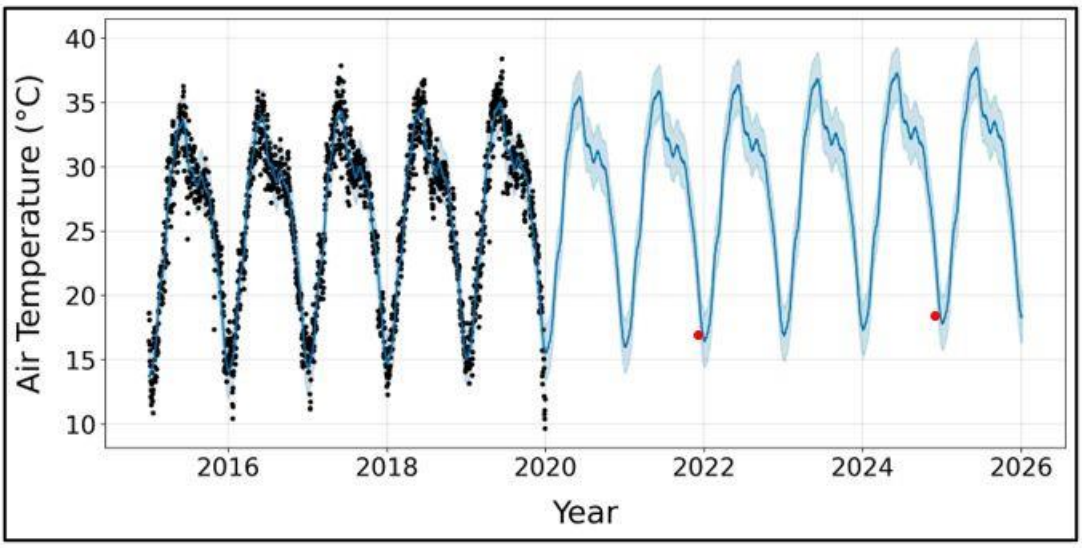

Figure 7.8 Prophet model predicted air temperature for the non-city river stretch

The prophet model gives better prediction results as it has a lower RMSPE value as compared to the SARIMA model. The RMSPE value has been calculated for the period of 2015 and 2020. The RMSPE value has been tabulated in table 7.4,

Table 7.4 RMSPE values showing the efficiency of Prophet and Sarima models

	RMSPE[a] (city)	RMSPE[a] (non city)
Prophet	3.02	3.58
Sarima	7.54	7.63

[a] The values have been denoted in percentage (%)

7.4.3 LSTM model validation and the future trend prediction

7.4.3.1 Accuracy assessment of the LSTM model(s)

The LSTM model(s) have been used to predict the river temperature and nighttime radiance. The scatter plot has been used for the representation of the comparison between model-derived and satellite-derived values. The L-8 image of 14 December 2020 has been used to validate the river temperature model generated from the LSTM algorithm. The nighttime (avg_rad) parameter has been validated using 1 Jan 2021 image. The city river stretch has more satellite pixels in comparison to that of the non-city river stretch. The city river stretch has an area of 3.37 km^2 as compared to the 1.97km^2 area for the non-city river stretch. For the average nighttime radiance imageries, the city portion has been clipped with a bigger shapefile as compared to the non-city portion. The validation has been done separately for the city and non-city stretch. Figures 7.9 and 7.10 have shown the comparison between the model-derived and the satellite-derived datasets for the city and non-city stretch river temperature, respectively. Figures 7.11 and 7.12 have shown the comparison between the model-derived and the satellite-derived datasets for the city and non-city nighttime radiance, respectively.

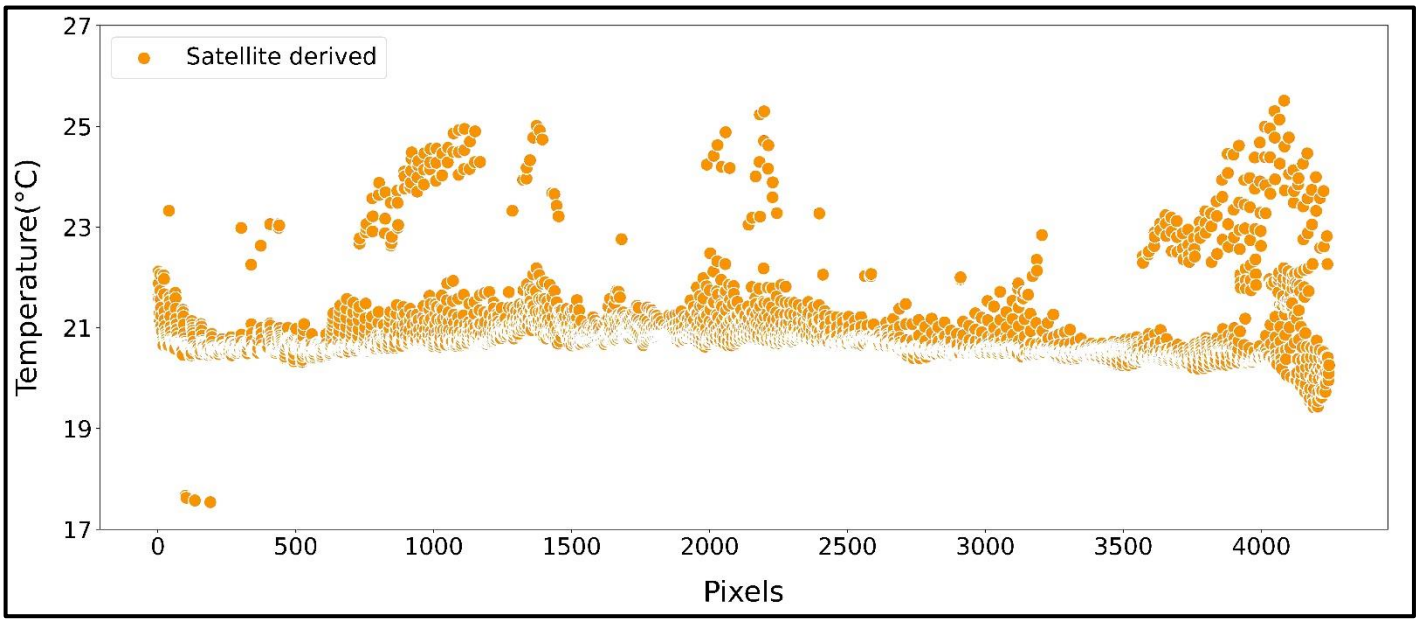

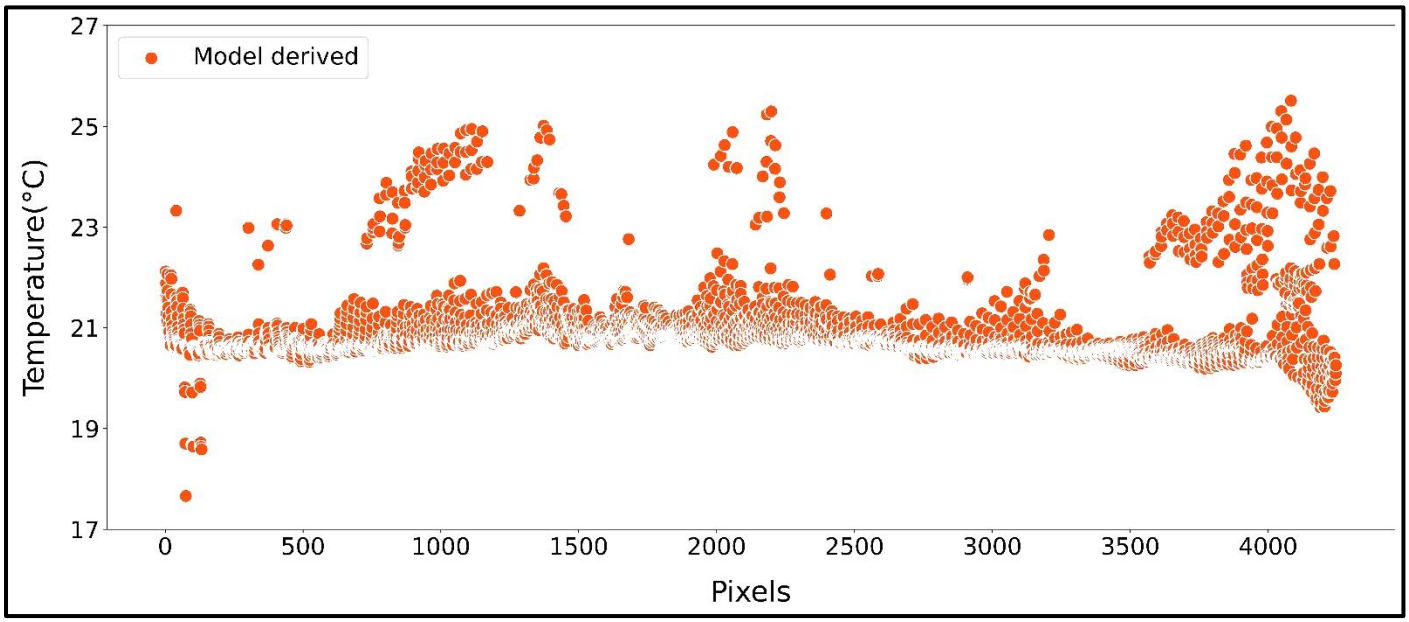

Figure 7.9 Comparison between the model derived and the satellite-derived datasets for the city stretch river temperature

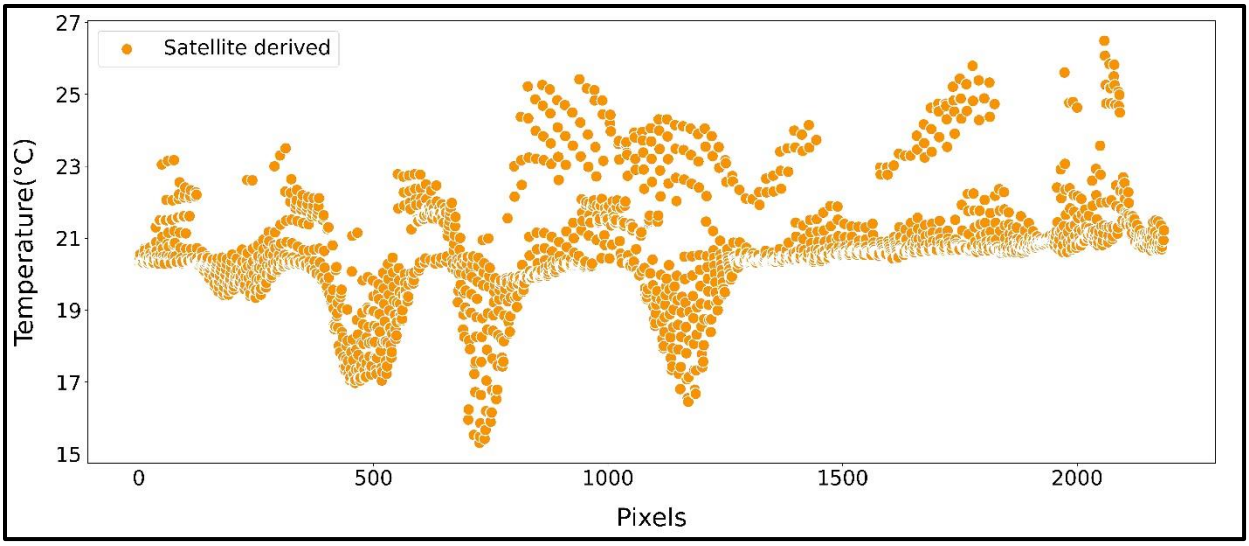

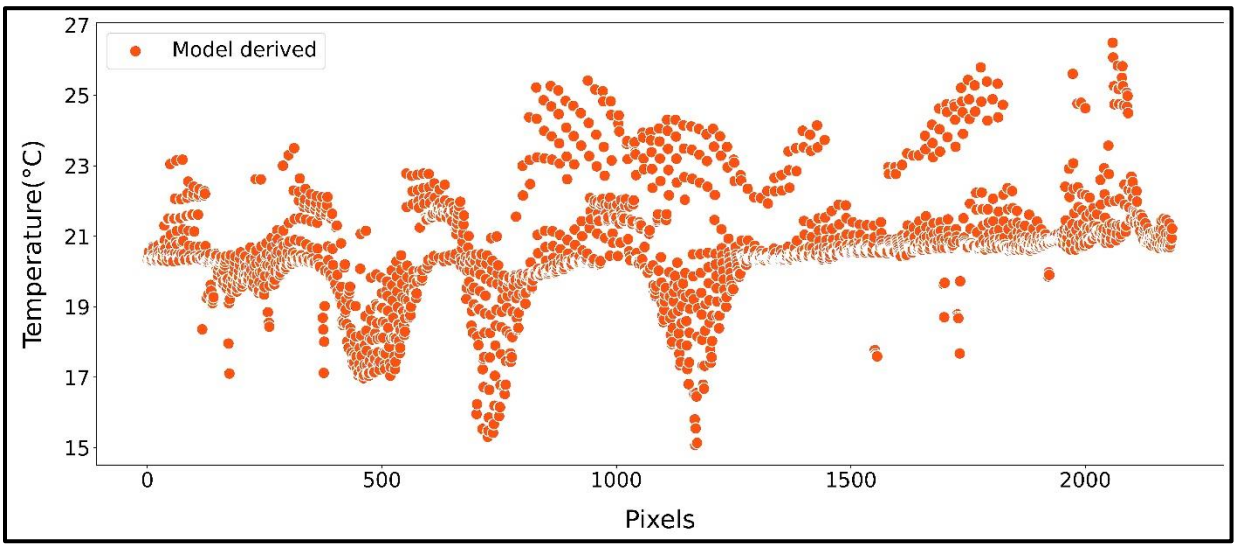

Figure 7.10 Comparison between the model derived and the satellite-derived datasets for the non-city stretch river temperature

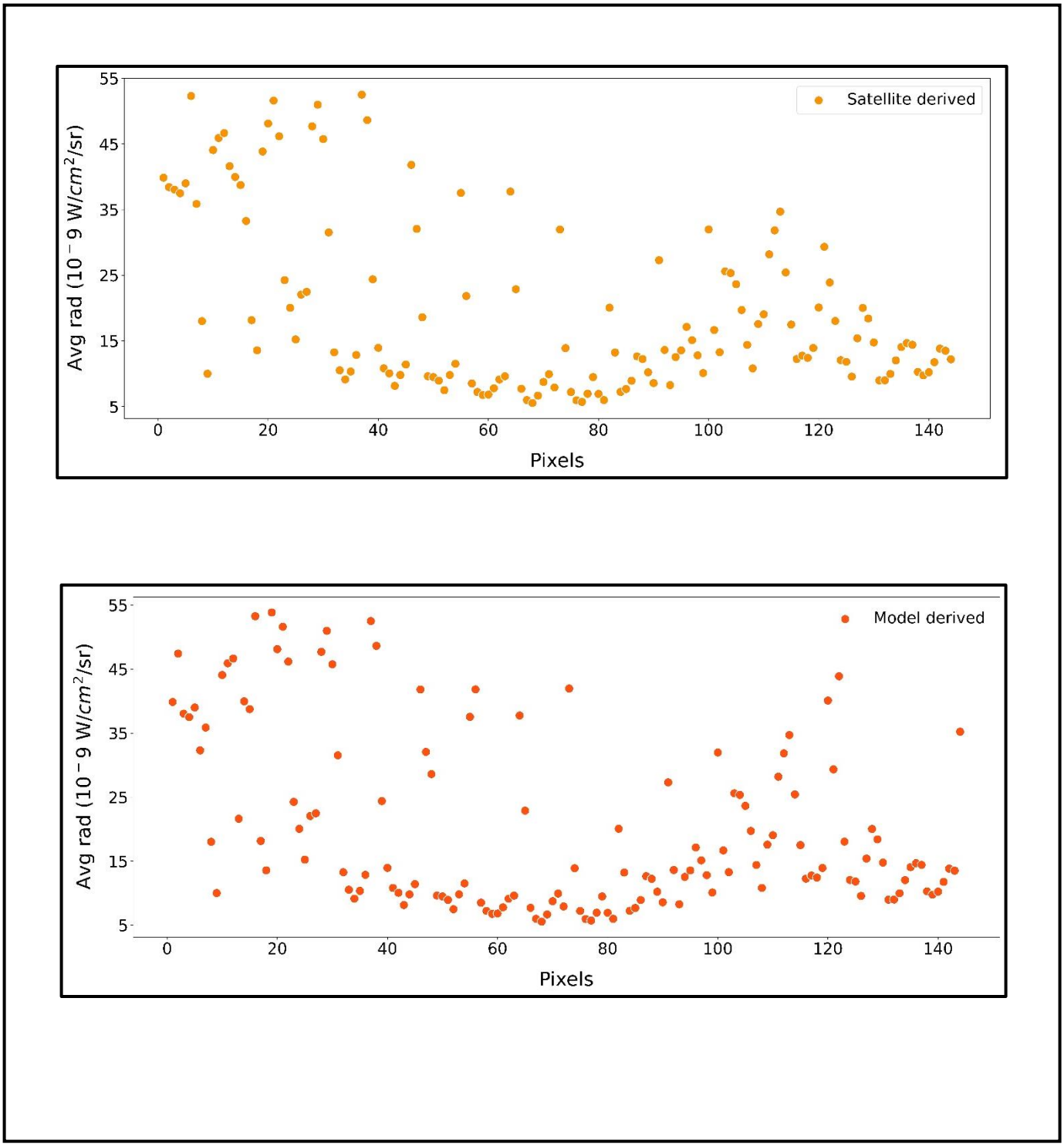

Figure 7.11 Comparison between the model derived and the satellite-derived datasets for the city nighttime radiance

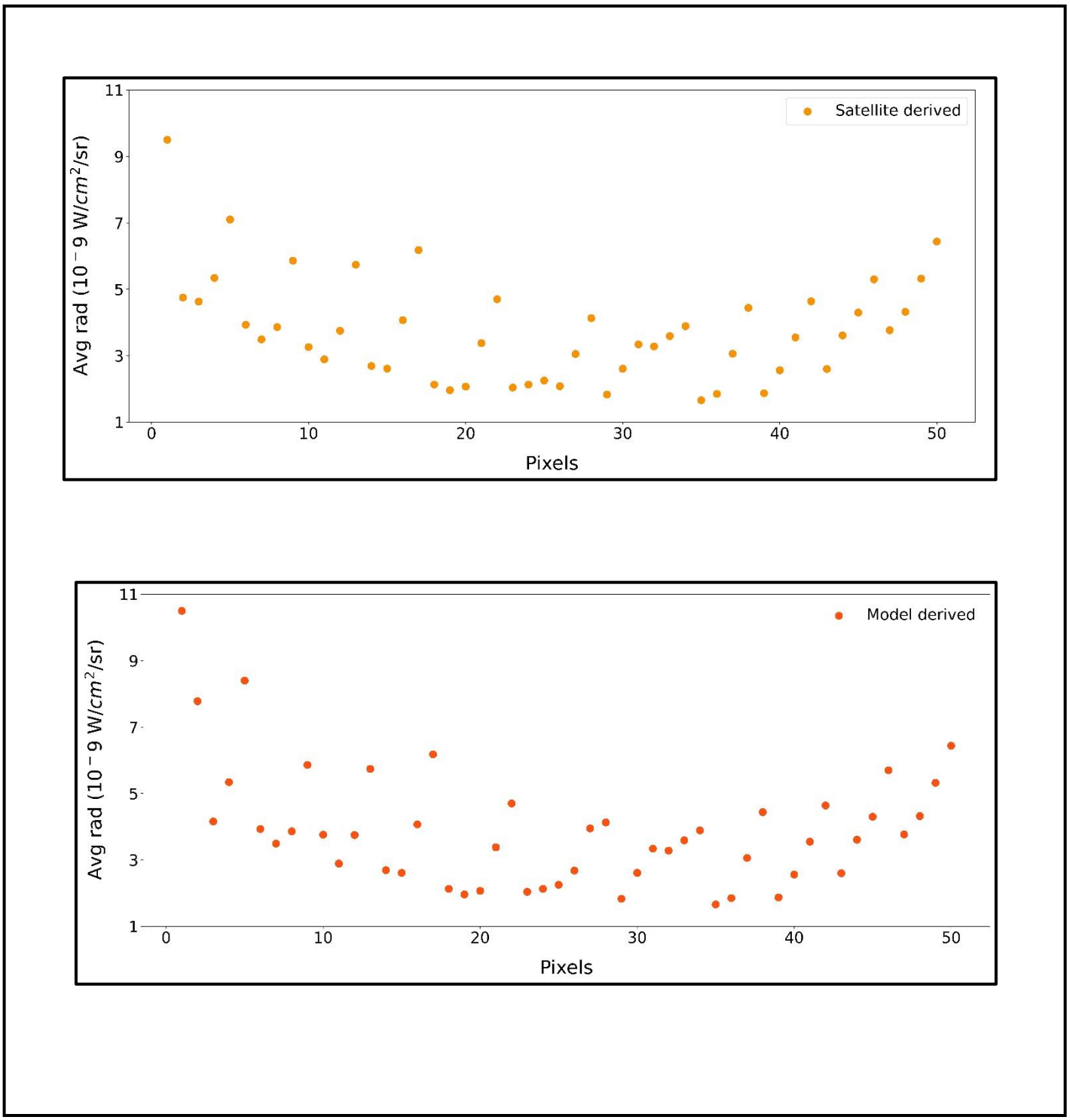

Figure 7.12 Comparison between the model derived and the satellite-derived datasets for the non-city nighttime radiance

The better R^2 (coefficient of determination) and lower RMSPE values have been observed for the river temperature as compared to the average radiance nighttime images.

Table 7.5 Performance analysis of the LSTM model(s)

	City		**Non-city**	
	R^2	**RMSPE[a]**	**R^2**	**RMSPE[a]**
River temperature	0.935	1.041	0.932	1.043
Nighttime average radiance	0.876	1.564	0.872	1.567

[a] The values have been denoted in percentage (%)

7.4.3.2 Future trend prediction

The river temperature has been predicted for the years 2022 and 2025. The prediction has been made separately for the city and non-city stretch river. There has been a difference of 1.96°C between the lower range of city stretch and non-city stretch river temperature. The uppermost temperature range has a difference of 0.06°C. For the city stretch, the average river temperature predicted by the model for 2022 has been 21.09°C, and for 2025 the average river temperature increases up to 21.67°C. Similarly, for the non-city stretch also, the same phenomenon has been observed. The mean river temperature has been 20.88°C for 2022, and for 2025 it increases to 21.51°C. Figures 7.13 and 7.14 shows LSTM predicted river temperature for the December 2022 and 2025 for city and non-city stretch, respectively.

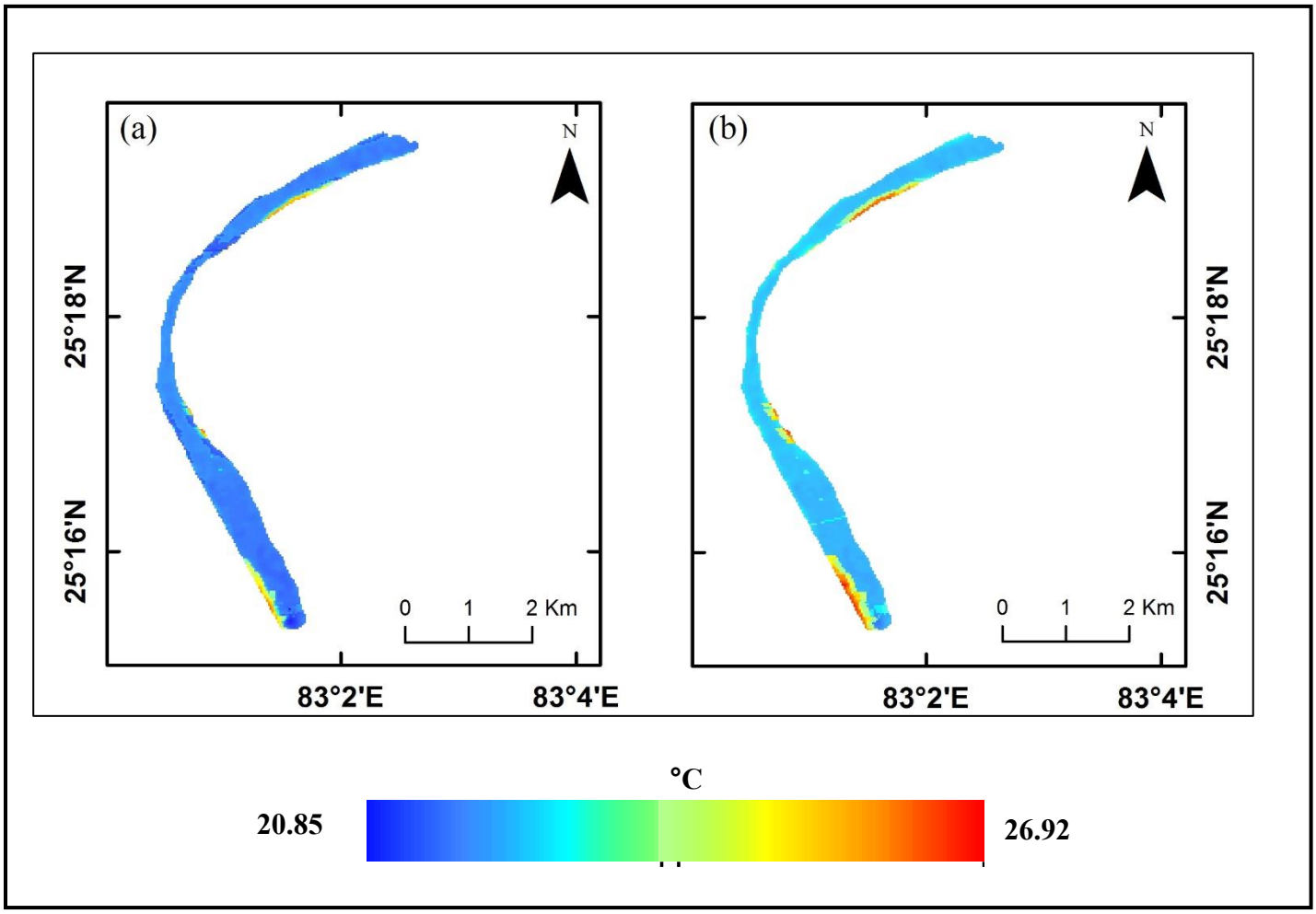

Figure 7.13 LSTM predicted river temperature for the city stretch for the year (a) 2022 (b) 2025

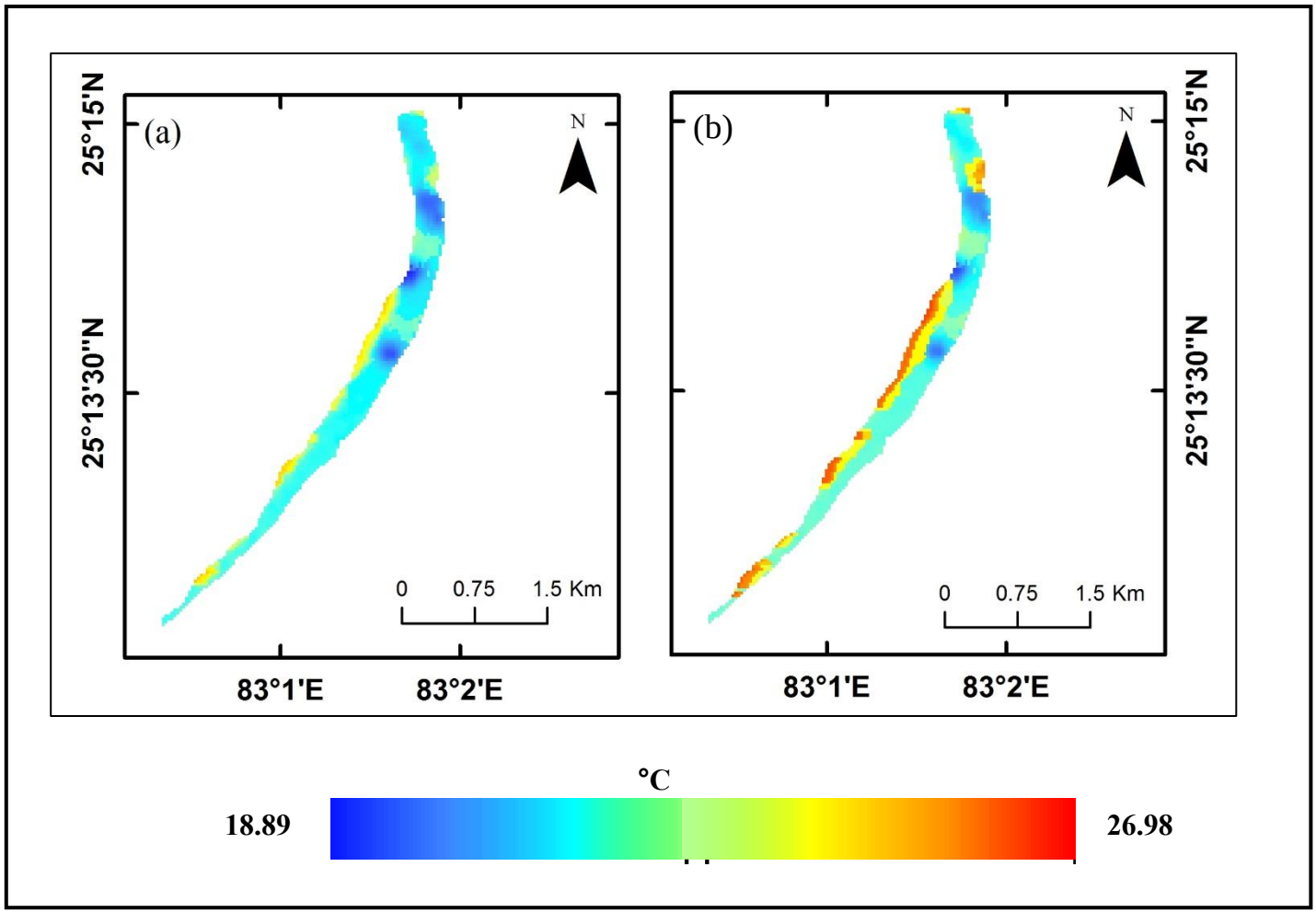

Figure 7.14 LSTM predicted river temperature for the non-city stretch for the year (a) 2022 (b) 2025

The nighttime average radiance for the surrounding region of the city river stretch shows significant fluctuation as compared to the non-city river stretch surrounding area. The mean of the 'average nighttime radiance' predicted by the model for the city river stretch surrounding region has been 18.82 nanoWatts/cm^2/sr for 2022 and 23.26 nanoWatts/cm^2/sr for 2025. Similarly, the area surrounding the non-city river stretch has also shown an increment in the mean value of the 'average nighttime radiance' but not as significant as compared to the surrounding area of the city river stretch. For 2022, the mean of 'average nighttime radiance' for the non-city river stretch surrounded region has been 5.95 nanoWatts/cm^2/sr and 9.83

nanoWatts/cm^2/sr for the year 2025 as predicted by the model. The overlaid shapefile (blue color) represents the river stretch in figures 7.15 and 7.16.

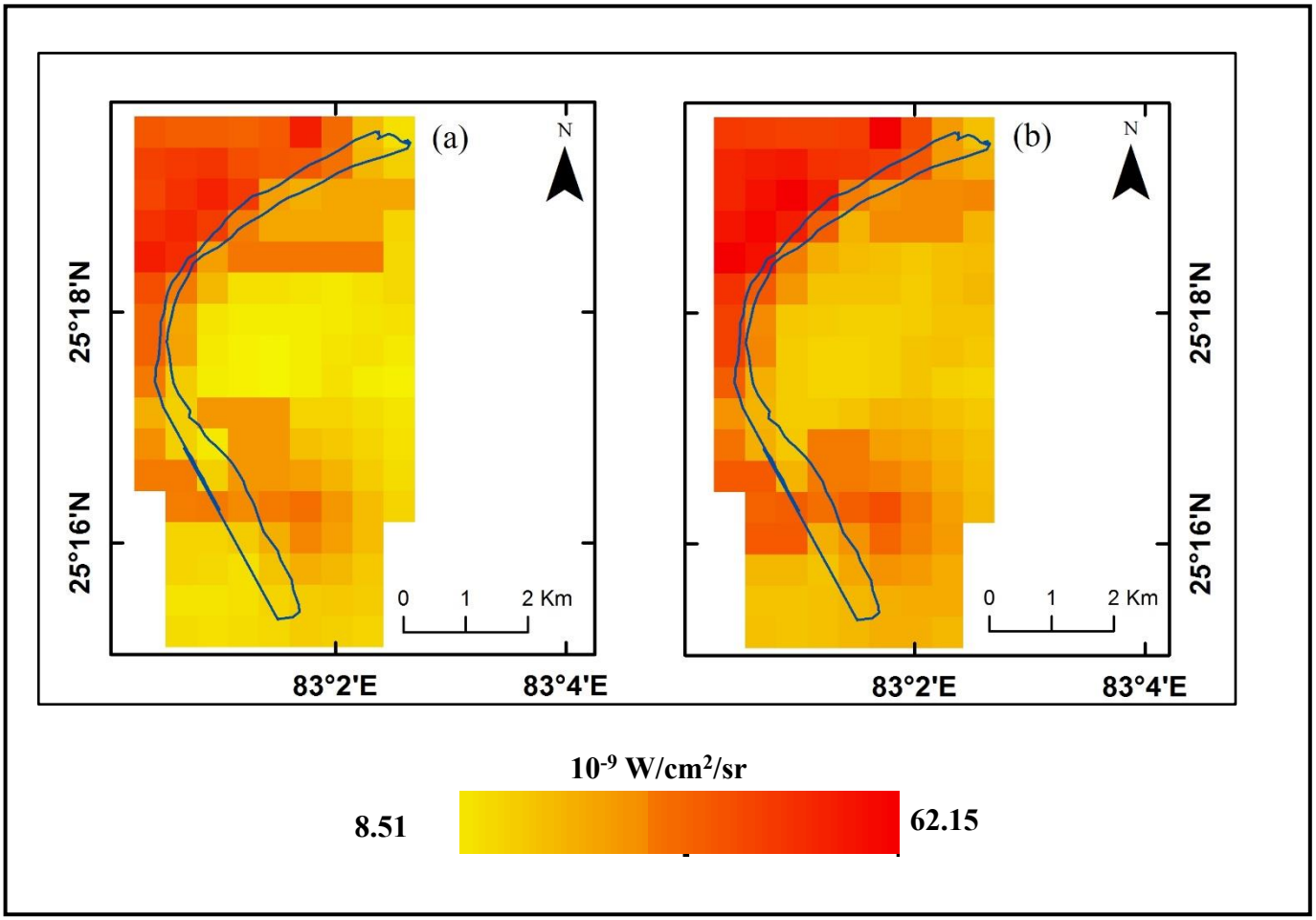

Figure 7.15 LSTM predicted nighttime radiance for the region surrounding the city river stretch for the year (a) 2022 (b) 2025

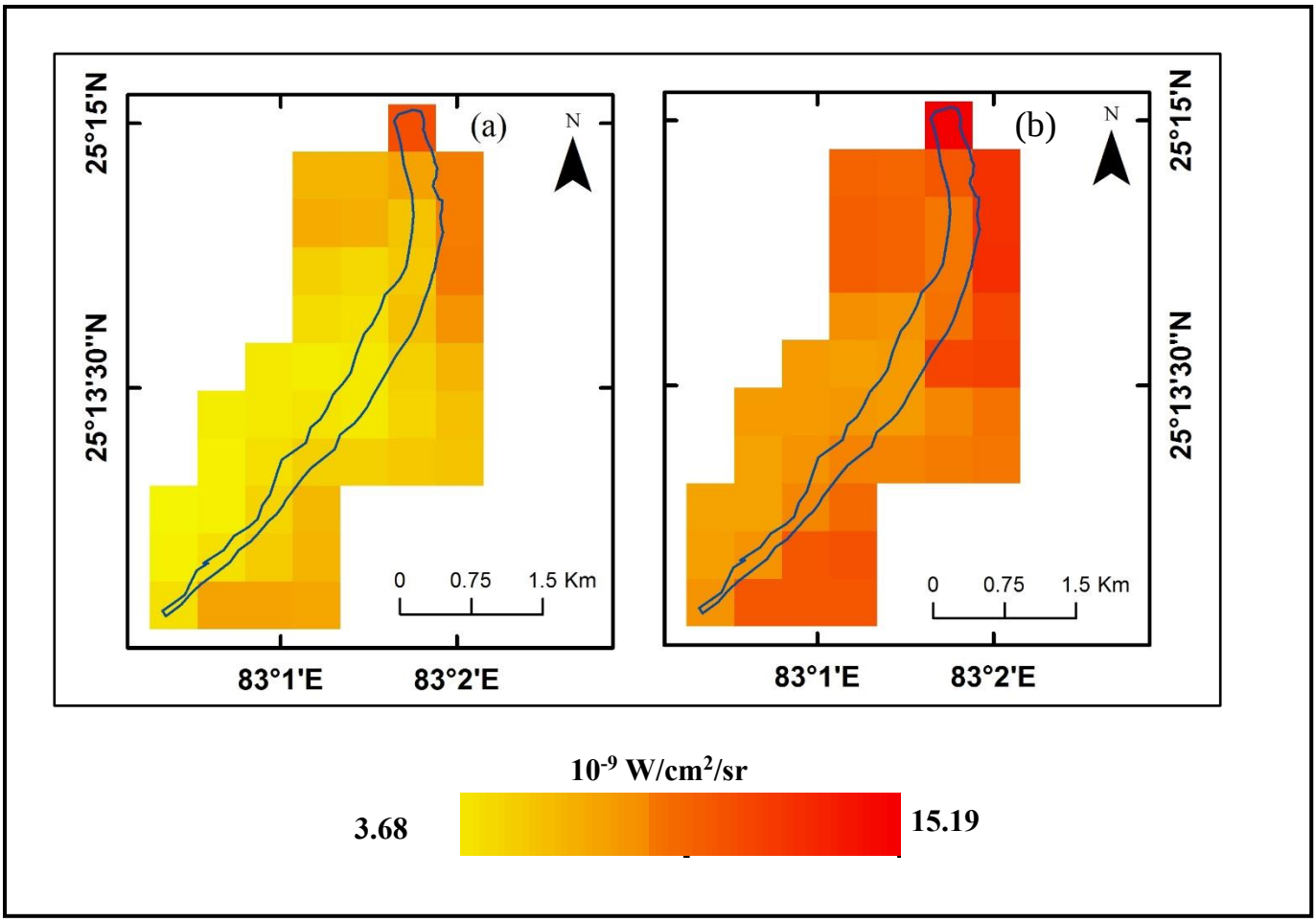

Figure 7.16 LSTM predicted nighttime radiance for the region surrounding the non-city river stretch for the year (a) 2022 (b) 2025

The p-value for the model-generated output has been less than 0.05. For this analysis, the significance level has been set to be more than 95%. For the average nighttime radiance parameter, the significance level has been lowest among all the parameters. All the parameters have shown a significance level of more than 95%. The p-value of the LSTM model(s) is shown in table 7.6.

Table 7.6 p-value of the LSTM model(s) for predicted years

	City (p-value)		Non-city (p-value)	
	2022	**2025**	**2022**	**2025**
River temperature	0.019	0.023	0.019	0.022
Nighttime average radiance	0.029	0.034	0.031	0.037

7.5 Discussion

7.5.1 Analysis of the elevated river temperature in the study stretch

In this analysis, the river temperature shows an increasing trend for the future years. From the study, it can be perceived that LSTM model(s) can be implemented for the time series prediction. The deep learning techniques have better adaptability in learning non-linearity, especially in handling the geo-spatial datasets (Barzegar et al., 2020). The air temperature over the river stretches also illustrates the rising trend. The predicted December average air temperature was calculated approximately as 17°C for 2022 and 19°C for 2025. The increase in air temperature can be associated with the global warming effect. In the upcoming years, the rise in the air temperature can be much more worrying and dreadful (Diffenbaugh and Field, 2013). The air temperature has been considered one of the essential factors which can affect the stream temperature, and the increment in air temperature can also elevate the river temperature (Hadzima-Nyarko et al. 2014). The river temperature has been essential for regulating the nutrient cycle of the aquatic organism so that they can sustain themselves (Caissie, 2006; Wawrzyniak et al., 2011). If the stream temperature rises beyond an explicit

threshold, the growth of aquatic species witnesses a declining curve which can disrupt the river ecosystem (Eaton et al. 1995; Xin and Kinouchi, 2013). The growth rate of bacteria and phytoplankton will be badly influenced by the increased river thermal phenomenon, which will stimulate the procedure of eutrophication, thus causing the river quality to degenerate (Wade et al. 2002; Sakyi and Asare, 2012; Jain and Singh, 2020). The process of eutrophication hampers the DO and increases the BOD. The predicted average river temperature for the non-city stretch for 2025 has been higher than the predicted average river temperature for the city stretch. The river temperature in the city stretch also displays an increasing trend. The reasons can be attributed to the effect of anthropogenic activities. The urbanization of the city also infuses the effect of global warming (Maheshwari et al., 2020). The non-city part in 2025 has a higher temperature compared to the city part because of the sand bar intrusion in the non-city region. The river width at some places in the non-city region becomes extremely narrow due to the sand bar, and this can cause an elevation in the river thermal profile. Varanasi itself has been one of the densely populated cities in India. The nighttime average radiance has been analyzed in this study to dissect the effect of human intervention. The LSTM model has predicted an increase of 8.21 nanoWatts/cm^2/sr in the mean value of the December nighttime radiance for the surrounding city area in 2025 as compared to 2020. This indicates that anthropogenic activities will increase tremendously in the near future, and that can damage the river ecosystem. The anthropogenic effect will have a lesser influence on the non-city river stretch. The maximum value of nighttime radiance predicted by the model for the area surrounding the non-city river stretch has been 15.19 nanoWatts/cm^2/sr. Industrial waste consists primarily of heavy metals, which can increase the river temperature (Das et al., 2021).

Obviously, global warming and enhanced anthropogenic activities could endanger the sustainability of the river for this study region in the near future.

7.5.2 Impact of global warming on river Ganga and over the Ganga basin

The Ganga river basin has been considered India's most important river basin, and it has already been in the water stress zone (Singh and Kumar, 2018). The change in the climatic pattern due to global warming has a considerable impact on the dynamics of the river Ganga (Jain and Singh 2020). A significant portion of northern India will get directly affected, which depends on the river for agricultural, industrial, and domestic needs. The precipitation pattern also shows signs of variation due to climate change (Shrestha et al., 2017). The studies by researchers have shown that there have been mixed rainfall patterns. This uneven rainfall sequence may result in floods, and other extreme conditions like drought can also happen (Ghosh and Mistri, 2015). The river flow pattern also gets affected due to this irregular rainfall pattern, which can prove detrimental to the aquatic ecosystem along with the reduced DO in the river (Bocaniov et al. 2016). The inconsistent rainfall behavior enhances the evaporation rate, which contributes to the water table lowering. That will eventually lead to the depletion of the groundwater level in the region and low agricultural output, and inadequate soil productivity (Kumar 2012; Kidmose et al. 2013).

The feeding glacier of river Ganga, the Gangotri glacier, which is situated at Uttarkashi district of Garhwal Himalaya, has been retreating at a rate of 19m/year due to enhanced temperature and climate change (Naithani et al. 2001). The decomposition process gets intensified due to increased river temperature, which can be harmful to nutrient cycling (Jain and Singh 2020). Due to global warming and rising temperature, there will be massive variations in river water quality (Rehana and Mujumdar, 2011; Todd et al. 2012). The enhanced river temperature will

increase the growth rate of bacteria and phytoplankton, which in turn can aggravate the eutrophication process, thus causing the river water quality to deteriorate (Wade et al. 2002; Sakyi & Asare 2012). In the warmer river water, the blue-green algae (cyanobacteria) can flourish (Daufresne and Boët, 2007) and that can be harmful to other aquatic organisms (Tare et al. 2003; Zanchett and Oliveira-Filho, 2013). Due to the rise in the air temperature because of the global warming scenario, the water temperature also increases. Climate change has affected all the levels of riverine biodiversity, from species to biome levels (Learmonth et al. 2006; Bellard et al. 2012). The loss of the aquatic habitat has been experienced mainly at those places where the river temperature depicts a higher rise (Eaton and Scheller,1996). Climate change also has very adverse effects on the specific biota of the River Ganga (Jain and Singh, 2020).

River Ganga has been an adobe to a number of reptiles, fish species, mammals, and birds. Endangered species such as the Gangetic Dolphin (*Platanista gangetica*), Ganges softshell turtle (*Nilssonia gangetica*), Gharial (*Gavialis gangeticus*), Himalayan Mahseer (*Tor putitora*), etc. have been already under severe threat. These species have been moving towards a higher extinction risk every passing year. The restoration of the Ganga river ecosystem can be possible if a vis-à-vis thermal pattern of the river ecosystem is studied in an intensive way.